Effects of Convective Solute and Impurity Transport in Protein Crystal Growth

Peter G. Vekilov,* Bill R. Thomas, and Franz Rosenberger

Center for Microgravity and Materials Research, University of Alabama in Huntsville, Huntsville, Alabama 35899

Received: September 26, 1997; In Final Form: December 16, 1997

High-resolution optical interferometry was used to investigate the effects of forced solution convection on the crystal growth kinetics of the model protein lysozyme. Most experiments were conducted with 99.99% pure protein solutions. To study impurity effects, ~1% of lysozyme dimer (covalently bound) was added in some cases. We show that the unsteady kinetics, corresponding to bunching of growth steps, can be characterized by the Fourier components of time traces of the growth rate. Specific Fourier spectra are uniquely determined by the solution conditions (composition, temperature, and flow rate) and the growth layer source activity. We found that the average step velocity and growth rate increase by ~10% with increasing flow rate, as a result of the enhanced solute supply to the interface. More importantly, faster convective transport results in lower fluctuation amplitudes. This observation supports our rationale for system-dependent effects of transport on the structural perfection of protein crystals. We also found that solution flow rates >500 μm/s result in stronger fluctuations while the average growth rate is decreased. This can lead to growth cessation at low supersaturations. With the intentionally contaminated solutions, these undesirable phenomena occurred at about half the flow rates required in pure solutions. Thus, we conclude that they are due to enhanced convective supply of impurities that are incorporated into the crystal during growth. Furthermore, we found that the impurity effects are reduced at higher crystal growth rates. Since the exposure time of terraces is inversely proportional to the growth rate, this observation suggests that the increased kinetics instability results from impurity adsorption on the interface. Finally, we provide evidence relating earlier observations of "slow protein crystal growth kinetics" to step bunch formation in response to nonsteady step generation.

1. Introduction

Protein crystals are currently predominantly used for molecular structure studies by diffraction techniques. Interest in convection effects on protein crystallization has been stimulated by the finding that, in some cases, improved X-ray diffraction resolution has been achieved by growth in the reduced gravity environment on spacecraft.[1−4] Several scenarios for improvements in protein crystal perfection under reduced gravity have been put forth; for discussion and references see ref 5. Some of the disadvantages of growth under normal gravity, e.g., sedimentation of particulate matter and newly nucleated crystallites on the growing surface, followed by stress-causing incorporation into the crystal,[6] can be avoided on earth by removal of soluble and particulate impurities from the solutions and by growth under supersaturations lower than those required for secondary nucleation. Another consequence of gravity is the solution flow caused by density gradients in the solution. Under isothermal conditions, such gradients are mostly due to the depletion of solute around the growing crystals. The velocity of these buoyancy-driven flows has been both experimentally and numerically estimated to be of the order 10 μm/s for lysozyme crystals growing at about 100 Å/s.[7,8] The reduction of buoyancy-driven convection in space results in lower interfacial supersaturation and lower growth rate. This has been speculated to be advantageous for crystal quality.[4,9] The general validity of this expectation has been questioned on the basis of experimental evidence for an optimal supersaturation range for the growth of more perfect proteins crystals.[10,11] This is not surprising, since, as shown for some inorganic crystals, defect formation can be stronger at low growth rates.[12−15] Furthermore, slower convection has been suggested to lower the interfacial concentration of impurities that are incorporated into the crystal.[5] Thus, the role of convective solute and impurity transport in protein crystal growth and its effects on crystal perfection merit detailed investigation.

In our earlier work, employing a high-resolution laser interferometry technique with digital image and signal processing,[16] we found with the model protein lysozyme that under steady solution conditions the growth rate, step density, and step velocity can fluctuate by as much as 80% of their average values.[17] The step density variations indicate that the rate unsteadiness occurs through the dynamic formation of step bunches (macrosteps). Our studies of these defect-causing fluctuations resulted in the basic conclusion that they represent an intrinsic instability of the growth process under mixed surface kinetics and bulk-transport control.[17−19] On the basis of these considerations, one expects the strongest instability (highest fluctuation amplitude) to occur in processes that operate under equal weight of the transport and kinetics in the overall rate control. Hence, we concluded that shifts of the crystallization conditions to either pure kinetics or transport control should result in more steady growth. This hypothesis provides, for the first time, a system-dependent rationale for the advantages as well as the disadvantages of variations of transport conditions for (protein) crystal perfection.

* To whom correspondence should be addressed. E-mail peter@cmmr.uah.edu, fax (256) 890-6791.

S1089-5647(97)03123-4 CCC: $15.00
Published on Web 06/06/1998

To date, the above hypothesis has been supported by numerical simulations[20] of the coupled transport and interfacial kinetics processes in a system representative of lysozyme crystallization which is dominantly controlled by interfacial kinetics. The model quantitatively reproduces the experimentally observed kinetics unsteadiness. Furthermore, on change of the governing parameters toward stronger kinetics control or higher nonlinearity in kinetics, the simulations yield respectively a decrease and increase in the fluctuation amplitude, as expected from the above instability considerations.

In this paper we present further studies of the growth kinetics unsteadiness employing forced solution flow. According to the above rationale, faster convective solute transport to the interface shifts the operating point of the system toward stronger kinetics control and should thus result in lower kinetics fluctuations. Since these studies involve comparisons of unsteady kinetics traces, we first define and test a method of reduction of the complex unsteady kinetics data to characteristic sets, based on Fourier decomposition. We use the Fourier spectra to quantify the changes in unsteady kinetics with flow velocity. With increasing solution flow rate we obtained the predicted decrease in fluctuation amplitude. Yet, quite unexpectedly, at even higher flow rates the fluctuation amplitudes increased again. This was accompanied by significant suppression of growth, up to growth cessation at low supersaturations. Experiments performed with highly purified lysozyme and after the addition of 1% lysozyme dimer (the most common impurity for this protein)[21] unambiguously correlate the amplitude increase and growth deceleration with enhanced impurity transport to the crystal−solution interface.

2. Experimental Procedures

The interferometric and computer imaging subsystems used here were as described earlier.[16] Interferometric intensity traces were recorded at select locations on the crystal surface, as well as from reference spots on the crystallization cell bottom. The processing of the traces to obtain the local displacements of crystal facets due to growth, and from these the local values of normal growth rate, vicinal slope, and tangential step velocity, remained also unchanged.[16] All solutions used here contained 50 mg/mL lysozyme from hen egg white, 2.5% (w/v) NaCl as a precipitant, and 0.05 M acetate buffer ($NaCH_3COO-CH_3COOH$) to fix the pH at 4.5. Lysozyme of 99.99% purity was used, prepared as described in ref 21. To study impurity effects, in some runs covalently bound lysozyme dimer was added at ~1% (w/w dry protein) to a solution of the purified material. This dopant concentration corresponds to the dimer concentration in lysozyme supplied by Seikagaku.[21] The dimer was extracted from samples of purified lysozyme oxidized with H_2O_2 (for details, see ref 22), and its concentration in the crystallizing solution was verified by gel electrophoresis with high-sensitivity silver staining[21] (gels not shown).

A novel crystallization and solution circulation system, consisting of a crystallization cell, peristaltic pump, and a reservoir, was developed for the present investigations. This system allows solution flow through the cell with velocities (measured at distances of a few crystal dimensions form the crystal) that can be varied in the range from 20 μm/s, comparable to the buoyancy-driven convection velocities, up to 2000 μm/s to amplify possible convection effects. The mechanical sturdiness of the overall arrangement allowed in situ high-resolution interferometric measurements during solution flow. Further details on the design, and extensive tests performed with this setup, are provided in ref 23.

Both {101} and {110} faces of tetragonal lysozyme crystals were studied. The results differ only in the specific values of some threshold parameters found with the two faces; see section 4.1.

3. Characterization of Unsteady Kinetics by Fourier Decomposition

3.1. Definitions. In a previous paper,[17] we used triplets of locally recorded time traces of the normal growth rate R, vicinal slope p, and tangential step velocity v to characterize the unsteady growth kinetics. These time traces are unique for each period of observation even on the same crystal face under steady external solution conditions (composition, temperature, and flow rate). Thus, monitoring of the flow velocity dependence of these unsteady kinetics would require unwieldy comparisons between a large number of such triplets. To simplify this analysis, a transformation and reduction of the $R(t)$, $p(t)$, and $v(t)$ traces to characteristic data sets is needed. The observed reproducibility of the time scales and amplitudes of deviation from the average values under identical external conditions suggests Fourier decomposition as a suitable means of data reduction. For this, we chose the Fourier representation

$$R(t) = \sum_n R_n \exp\left(\mathrm{i}\frac{2\pi n}{T}t\right) \tag{1}$$

where R_n and $2\pi n/T = f_n$ are the nth ($n = 0, \pm 1, ...$) complex Fourier amplitude and frequency, respectively. Using the representation

$$R_n = (A_n/2)\exp(\mathrm{i}\varphi_n) \tag{2}$$

with $A_n/2$ being the magnitude and φ_n the phase of the complex amplitude, (1) becomes

$$R(t) = \sum_n \frac{A_n}{2}\exp\left[\mathrm{i}\left(\frac{2\pi n}{T}t + \varphi_n\right)\right] \tag{3}$$

Since $R(t)$ is real, for all n

$$A_n = A_{-n} \tag{4}$$

Thus, we get

$$R(t) = \sum_n A_n \cos\left(\frac{2\pi n}{T}t + \varphi_n\right), \quad n \geq 0 \tag{5}$$

This form of the Fourier transform has the advantage that the $A_n = |R_n|$ can be calculated from any discrete set of growth rate measurements by using the accelerated algorithm of the fast complex Fourier transform.[24] Application of such accelerated algorithms to compute the amplitudes of the real Fourier series is limited to data sets of power 2^j, where j is a positive integer, or requires data extensions that are prone to errors.

Figure 1a,b presents an experimentally recorded $R(t)$ trace and its Fourier spectrum $A(f_n)$. For comparison, in Figure 1a we also show the $R(t)$ restored using (5) from the sets of $A(f_n)$ and φ_n (not shown). The good correspondence between the original and the restored traces indicates that the Fourier transform defined by (5) is an adequate representation of the unsteady growth rate. The slight deviations are likely due to the approximations assumed in the accelerated numerical algorithms for $R(t) \rightarrow A(f_n)$ and $A(f_n) \rightarrow R(t)$.

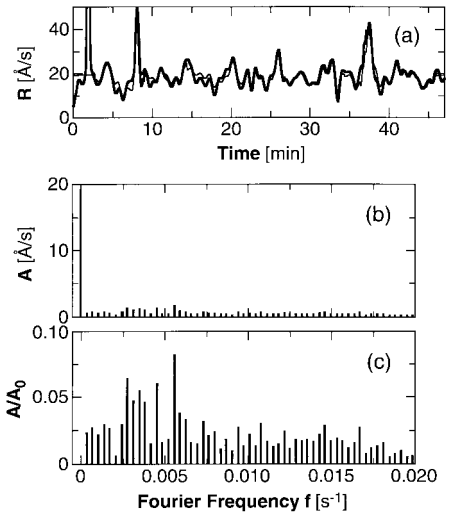

Figure 1. Illustration of the Fourier decomposition. (a) Thick line: normal growth rate trace $R(t)$ recorded on a (101) face at supersaturation $\sigma = 1.4$ and flow rate $u = 105$ μm/s; thin line: trace restored according to (5) from the Fourier spectrum $A(f)$ shown in (b). (c) Fourier spectrum normalized with respect to the averaged growth rate $R_{avg} = A_0$. $A/A_0 = 1$ at $f = 0$ is intentionally omitted.

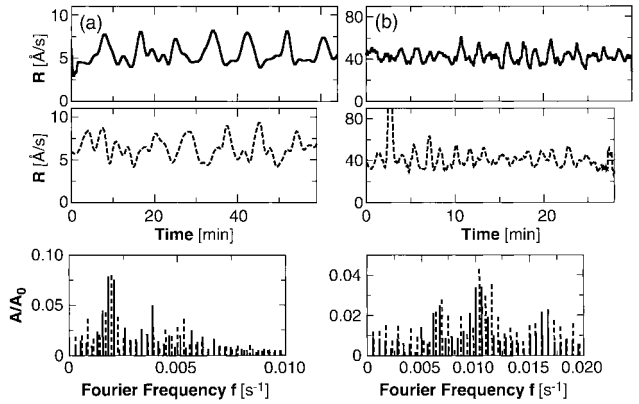

Figure 2. Comparison of Fourier spectra $A(f)/A_0$ corresponding to the two independent time $R(t)$ traces shown above the spectra. (a) Supersaturation $\sigma = 1.0$ ($T = 25$ °C), flow rate $u = 80$ μm/s, both traces recorded during growth of crystal A, between the shown traces the crystal grew at a different flow rate for ~30 min; (b) $\sigma = 1.4$ ($T = 22$ °C), $u = 105$ μm/s, traces recorded on crystals B and C during growth supported by similar dislocation groups as judged from vicinal slope and growth rate data.

In the decomposition defined by (5), all A_n have the dimension of R, length/time, and A_0 equals the growth rate averaged over the entire period of observation, R_{avg}. The normalized Fourier amplitudes A_n/A_0, shown in Figure 1c, represent the deviations from R_{avg} as a function of the frequency characteristic of each deviation. Furthermore, the Fourier frequencies defined above, are inversely proportional to the characteristic time scale Δt of the fluctuations. For instance, the maxima at $f = 0.0055$ s^{-1} in Figure 1b,c correspond to the fluctuations with a $\Delta t = 1/(0.0055$ s$^{-1}) \cong 180$ s $= 3$ min in Figure 1a.

3.2. Characteristic Nature of Transforms. Figure 2 presents two pairs of $R(t)$ traces and their respective Fourier spectra. The traces in Figure 2a were obtained at different times on the same crystal at the same solution conditions; see figure caption. The layers were generated by the same dislocation step source as judged by the origin and density of interference fringes; for details on step sources identification, see ref 25. The $R(t)$ traces in Figure 2b stem from two different crystals in other experiments under identical conditions, but different from those in Figure 2a. The layers were generated by sources of comparable activity, i.e., generating step trains with equal average density/slope. Note that, despite the apparent lack of correlation among the traces, the Fourier spectra of a pair are rather similar. However, comparison of parts a and b of Figure 2 shows that different combinations of solution conditions and step source activity result in different Fourier spectra; the contributions of these factors will be further analyzed in section 3.4.

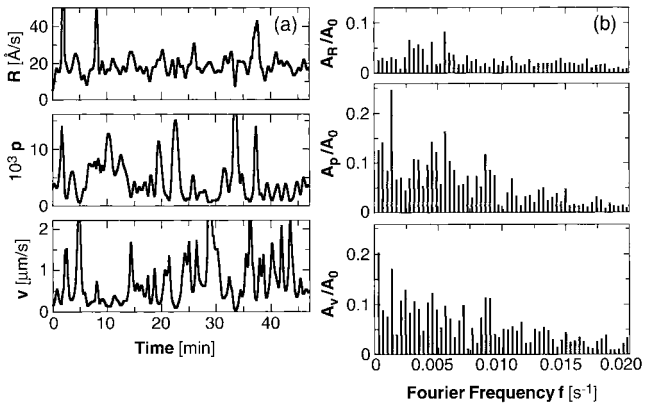

Figure 3. (a) Time traces of normal growth rate R, vicinal slope p, and step velocity v recorded on a (101) face at supersaturation $\sigma = 1.4$ and flow rate $u = 105$ μm/s. (b) Fourier transforms of the R, p, and v traces in (a).

Figure 2 presents but a small sample of numerous pairs of growth rate traces that we have analyzed and for which similar Fourier spectra were obtained provided that the growth layers were generated by sources of similar strength. Hence, we conclude that the Fourier spectra are fully determined by the external growth conditions and the growth layer sources and, thus, unambiguously characterize the growth rate unsteadiness as a function of these parameters.

3.3. Compatibility between the *R*, *p*, and *v* Spectra. Figure 3 compares the time traces of the growth rate R, vicinal slope p (proportional to local step density), and step velocity v and their Fourier spectra. The Fourier amplitudes of p and v are significantly higher than those of R (Figure 3b). This reflects the stronger fluctuations of p and v in Figure 3a. Since

$$R = pv \tag{6}$$

and the p and v fluctuations occur almost in counterphase, they largely balance to yield lower R fluctuations; for further discussion, see ref 17. The v and R spectra are uncorrelated. R and p spectra, on the other hand, show both similarities and differences. At $f \leq 0.001$ s^{-1}and $f \approx 0.0085$ s^{-1} the p spectrum has maxima that do not have corresponding R spectrum maxima. However, maxima at these frequencies are also present in the v spectrum. Due to the phase difference between p and v, these fluctuations compensate each other in the R trace. At all other frequencies, the spectra of R and p are similar: the maxima at $f \approx 0.003$, 0.0045, 0.0055, 0.011, 0.013, and 0.0145 s^{-1} are present in both. Since the p spectrum characterizes the fluctuations in step density, this correspondence indicates that the Fourier transform of the growth rate trace is also a reasonably good characteristic of step bunching. Consequently, in the remainder of this paper we will only use Fourier decompositions of $R(t)$.

3.4. Factors Affecting the Fourier Spectra. In Figure 2 we have seen that the Fourier spectra of $R(t)$ at two different supersaturations differ significantly. Since the average growth rate R_{avg} at these supersaturations is also different, it is nor clear

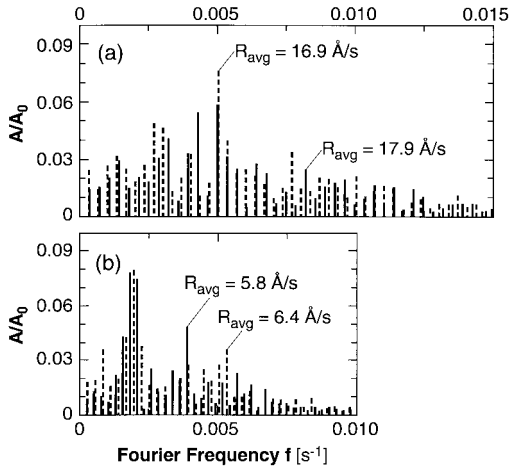

Figure 4. Fourier spectra $A(f)/A_0$ obtained at $\sigma = 1.0$ ($T = 25$ °C) and $u = 80$ μm/s: (a) crystal D, growing from a 99.99% pure lysozyme solution; (b) crystal A, same as in Figure 2a growing from a solution containing ~1% lysozyme dimer. R_{avg} for each series indicated on plots.

which of these two factors determines the Fourier spectrum. To distinguish between them, we show in Figure 4 the spectra corresponding to traces recorded at the same supersaturation $\sigma = 1.0$ and flow velocity $u = 80$ μm/s, but with different average growth rates due to different solution purity. Note that the maximum normalized amplitudes in Figure 4a,b are comparable. Interestingly, by dividing the f axis in Figure 4a by ~2, these spectra can be approximately scaled to those in Figure 4b. This scaling indicates that, in the cases discussed here, the higher impurity content does not introduce additional maxima in the Fourier spectra. (For results at higher flow rates, see sections 4.2. and 4.3.) This agrees with observations during growth in unstirred solutions that the characteristic amplitudes and time scales of the unsteady kinetics are independent of solution purity level.[17]

At the higher R_{avg}'s the spectrum is significantly shifted toward higher frequencies; i.e., the fluctuations occur on a shorter time scale. To rationalize this observation, we recall that, during growth with flowing solution, the concentration reaches its bulk value C at a certain distance δ from the interface.[26−28] This δ is largely determined by the flow velocity and does not depend on the growth rate R. On the other hand, the interfacial concentration is determined by the coupling of R to the concentration gradient dC/dz, higher R leading to steeper dC/dz. Since, as noted above, C at δ is independent of R, this means that the interfacial concentration C_s and supersaturation σ_s are lower.

Dimensional analysis indicates that the fluctuation frequency f should increase with increases of the normalized time derivative of R,

$$f \propto \frac{1}{R}\frac{\partial R}{\partial t} \approx \frac{1}{\sigma_s}\frac{\partial \sigma_s}{\partial t} \qquad (7)$$

For the approximate equality in (7), we use (17) from ref 17, where it was used to illustrate the relation between the local fluctuations in interfacial supersaturation and growth rate. Thus, the lower σ_s associated with higher R's lead, according to (7), to higher fluctuation frequencies and shorter time scales.

Note that the above considerations are strictly valid only for growth in flowing solution. In unstirred solutions in earth's gravity, δ is determined by the rate of buoyancy-driven convection and decreases with increasing R_{avg}.[29] This may result in smaller decreases in σ_s and to smaller variations of f with R_{avg}. On the other hand, during quasi-steady growth with purely diffusive transport under reduced gravity, δ equals the container dimensions, and this may again result in strong $f(R_{avg})$ dependence.

In our previous work dealing with experiments in unstirred solutions, we related the fluctuation time scale to a characteristic transport time τ_D in the system.[17] This τ_D depends on δ. Since, as pointed out above, in unstirred solutions δ depends on the growth rate, we assumed that the only effect of R_{avg} on f is through this dependence. Now we see that, even at constant δ, f is a function of R_{avg}.

We have shown above that similar Fourier spectra are obtained under identical solution conditions only if the growth layer source activity is comparable. If the growth layer source changes during a measurement, this leads to a different Fourier spectrum; see section 4.3 and ref 30. Furthermore, the Fourier spectra are alike within a step train generated by a specific growth layer source on the face, independent of the distance between the probe location and this source; for further discussion of flow effects on the step bunching evolution along the step path, see ref 31. This means that the step train preserves the information about the layer source and the perturbations that it introduces.

The dependencies of the Fourier spectra on R and on the growth layer source provide further support for the conclusion that the fluctuations and step bunching are not merely a transport- or kinetics-determined growth feature but represent the response of the system of coupled transport and interfacial processes to perturbations in step density generated by the growth layer source.

4. Results and Discussion

4.1. Dependence of the Fourier Spectra on Solution Flow Rate. Figure 5 presents, for three different flow rates, sets of growth rate and vicinal slope traces together with the Fourier transforms of R. In comparing parts a and b of Figure 5, we see that with forced solution flow the fluctuation amplitudes and step bunching first decrease. This agrees with our predictions for systems growing in the mixed regime with higher relative weight of interfacial kinetics (see Introduction). However, quite unexpectedly, Figure 5c shows that at still higher flow rates the growth rate fluctuation amplitudes and step bunching increase.

This behavior is illustrated in more detail in Figure 6, which shows the dependence of the Fourier spectra of $R(t)$ at two different supersaturations on the flow velocity in the range 0−1600 μm/s. These spectra indicate that an optimal flow rate exists at which the fluctuation amplitudes possess a minimum. At both supersaturations shown here, this minimum is reached at $u \approx 400$ μm/s. Similar studies performed with both (110) and (101) faces of about 10 crystals growing from different solution preparations revealed that (a) the flow rate at which minimal fluctuation amplitudes are reached is slightly lower (≈350 μm/s) on the (110) faces than on the (101) and (b) during growth from solutions prepared from material purified more than a month before the kinetics measurements this optimal value is shifted toward lower u's. Gel electrophoresis analyses revealed that, within such periods, lysozyme dimer is produced in concentrations of the order 0.1%.[22] Our previous crystal growth and nucleation studies have shown that this dimer acts as an impurity that impedes the growth of lysozyme crystals.[5,21]

For further characterization of this high flow rate effect, we compared the changes in the fluctuation amplitudes to the changes in the average values of R and v. In Figure 7, individual

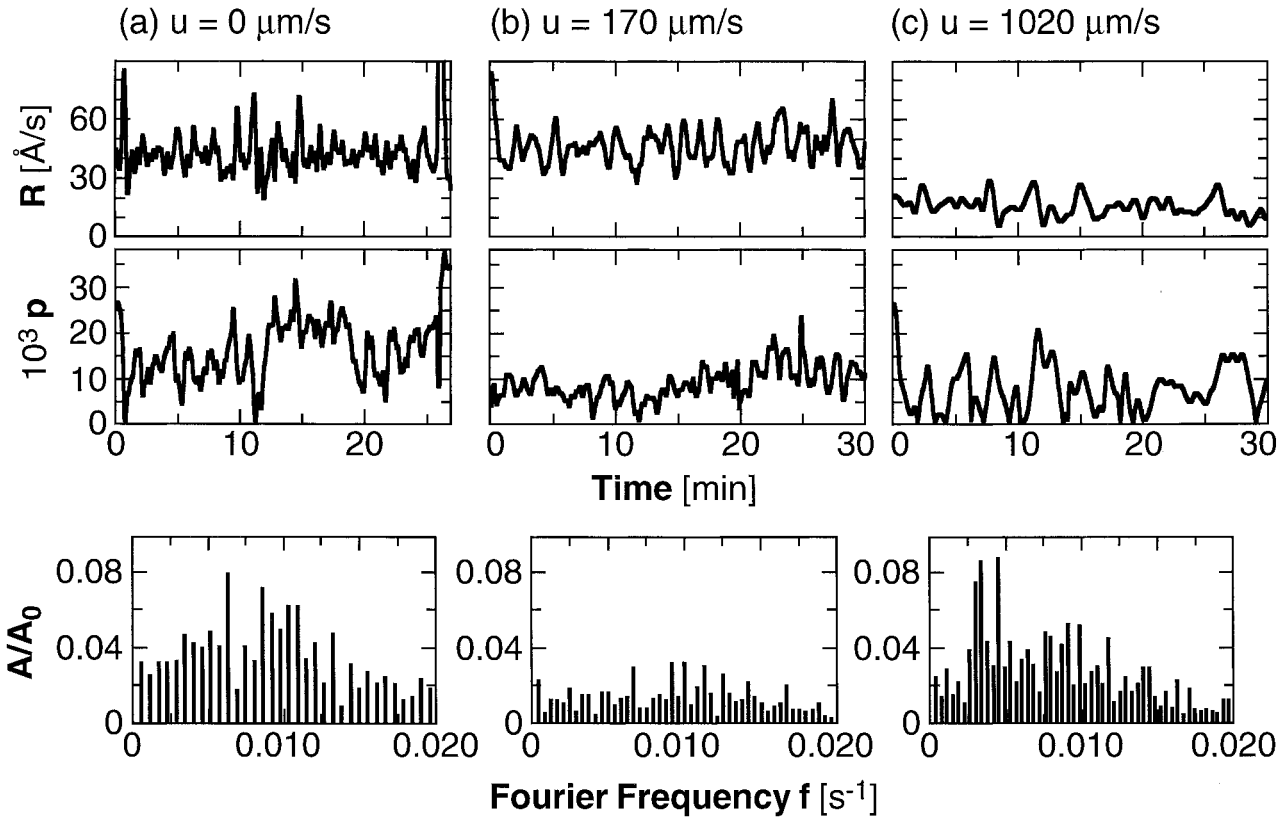

Figure 5. *R* and *p* traces and Fourier spectra of *R* recorded on a (101) face during growth from 99.99% pure lysozyme solution at $\sigma = 1.4$ ($T = 22$ °C). Forced flow rate *u* indicated on plots.

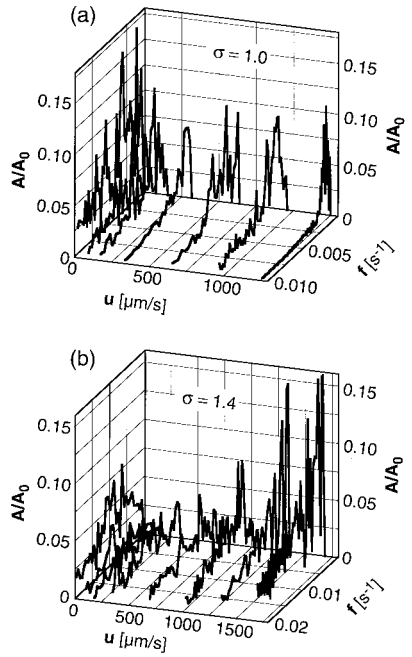

Figure 6. Fourier spectra $A(f)/A_0$ of growth rate traces during growth from 99.99% pure lysozyme solution as a function of flow rate *u*. (a) $\sigma = 1.0$, (b) $\sigma = 1.4$.

Fourier spectra at a specific flow rate are represented by the maximum amplitude observed. At the higher supersaturation $\sigma = 1.4$, *R* and *v* accelerate by about 10% on increasing *u* to ~200 μm/s and then monotonically drop to low values at higher flow rates. At the lower $\sigma = 1.0$, no initial growth acceleration is observed. Again, at $u = 300$ μm/s *R* and *v* decrease and at $u > 1300$ μm/s growth ceases completely. The initial acceleration of *R* and *v* at the higher supersaturation can be understood

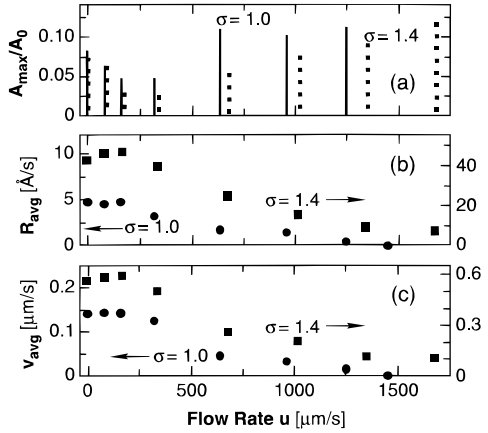

Figure 7. Variations with flow rate *u* of (a) maximum Fourier amplitudes A_{max}/A_0 extracted from the data in Figure 6; (b) average growth rate R_{avg} during the monitoring of the traces whose Fourier spectra are displayed in Figure 6; (c) the respective average step velocities v_{avg}. Supersaturation σ indicated at respective data in plots. Note the different scales of $R_{avg}(u)$ and $v_{avg}(u)$ for the two supersaturations.

in the following terms. Scaling analysis,[32,33] numerical simulations,[8] and interferometric measurements with lysozyme[34,35] have revealed that, during growth from unstirred solutions at rates of about 50 Å/s, the interfacial supersaturation is approximately 10% lower than the bulk supersaturation. Forced solution flow of sufficient strength overcomes this depletion. Thus, the increase in *v* and, hence, *R*. At the lower supersaturation, at which the average growth rate at $u = 0$ is about an order of magnitude lower, the interfacial solute depletion in unstirred solution is significantly lower. Thus, the solution-flow-induced growth acceleration is not noticeable.

The decrease of step velocity and growth rate at higher flow

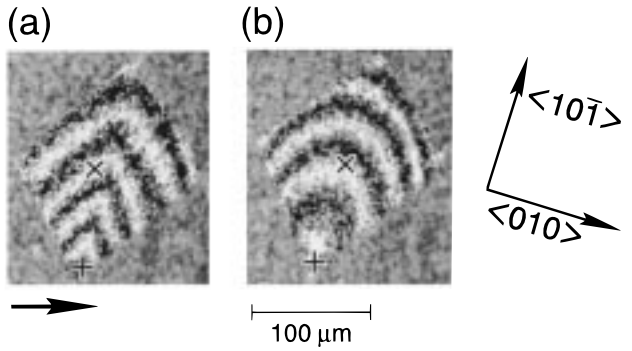

Figure 8. Morphologies of the facet during the recording of the traces used for the Fourier spectra in Figure 9. Supersaturation $\sigma = 1.4$ ($T = 22$ °C), flow velocity $u = 105$ μm/s in direction indicated by arrow (a) growth from 99.99% pure lysozyme solution; (b) after addition of 1% covalently bound lysozyme dimer. +, location of layer generation; ×, location of growth kinetics monitoring.

rates, and the dependence of optimal flow rate for minimal fluctuations on the solution age and the facet crystallographic orientation, suggest that these phenomena are due to flow-enhanced transport of growth-inhibiting impurities to the interface. This requires that the impurity is at least partly incorporated into the crystal during growth and that its diffusivity is sufficiently low such that its concentration at the interface is lower than in the bulk solution. Only then can enhanced, convective transport increase the interfacial impurity concentration.

The higher interfacial concentration of impurities may lead to stronger step bunching and growth rate fluctuations according to various mechanisms.[12,36,37] A common requirement is that the characteristic time of impurity adsorption is comparable to the terrace exposure time, which, in turn, is inverse proportional to R. In section 4.2 we will test the applicability of the impurity action mechanism; evidence for growth-rate dependent impurity effects will be provided in section 4.3.

4.2. Enhanced Impurity Transport Effects on Kinetic Fluctuations. In previous studies we have found that the lysozyme step velocities strongly depend on the concentration of impurities (dimer and other proteins)[25,32,33] and that lysozyme dimers are weakly segregated at the growing interface.[22] Based on the dimer size, it is safe to assume that its diffusivity in the solution is lower than that of the monomeric solute. Thus, the above mechanism of the increased fluctuations at higher flow rates is feasible. For tests of this mechanism, we first investigated the dependencies of Fourier spectra on u at two supersaturations using the high-purity solution. Then we added ~1% lysozyme dimer to the solution and observed the changes that this introduced to the $A/A_0(f)$ dependence on u during the growth of the same crystal.

Figure 8 compares the morphology of the dislocation growth hillock before and after the impurity addition. In both cases the steps are generated at the lower corner of the facet and propagate upward. We see that, upon the addition of dimer, the 2D anisotropy of the growth features disappears and the hillock becomes rounded. Since this hillock anisotropy is determined by the anisotropy of step velocity, this observation can help us to decide between the two possible impurity actions on the step kinetics: (a) adsorption at kinks on steps that decrease the kinetic coefficient and decelerate steps at all supersaturations[27,38,39] and (b) impurity adsorption on the terraces between steps that slows down steps only at supersaturations at which the critical 2D radius is greater than or comparable to the average impurity interparticle distance.[40] The second

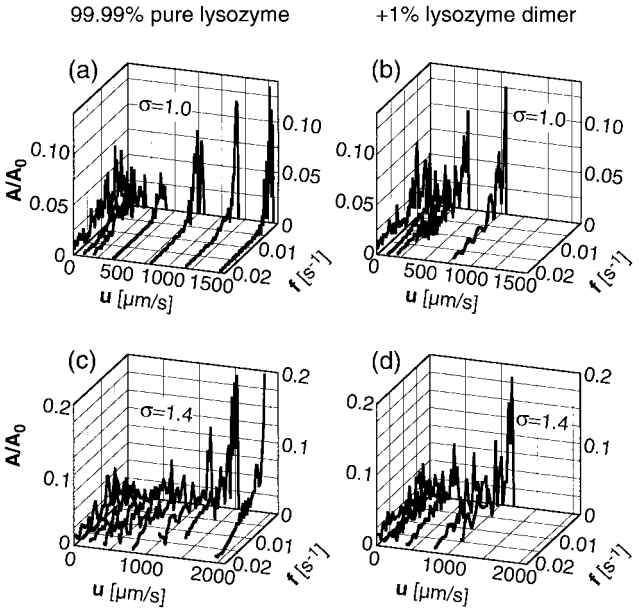

Figure 9. Fourier spectra $A(f)/A_0$ of growth rate traces obtained at two supersaturations as a function of flow rate u during growth from solutions before and after the addition of ~1% lysozyme dimer to 99.99% pure lysozyme. Note the different u-axis range in (a) and (b) as compared to (c) and (d).

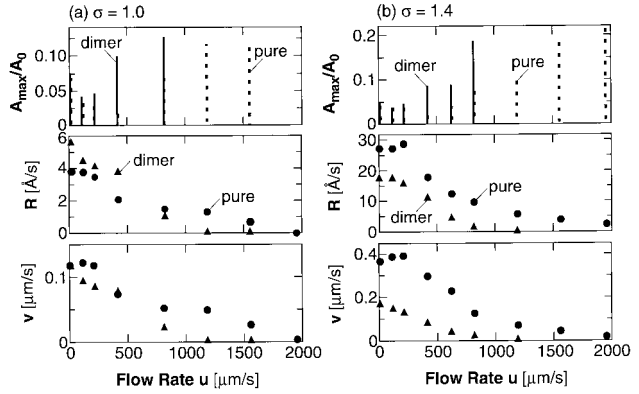

Figure 10. Flow rate dependence of variations of maximum Fourier amplitudes A_{max}/A_0 at two solution purity levels extracted from the data in Figure 9, average growth rate R_{avg} and average step velocities v_{avg} during the monitoring of the traces whose Fourier spectra are displayed in Figure 9. (a) $\sigma = 1.0$ ($T = 25$ °C), (b) $\sigma = 1.4$ ($T = 22$ °C).

mechanism likely leads to step deceleration independent of propagation direction and, thus, to no change in step anisotropy. Hence, we conclude that the dimer is preferentially adsorbed at kinks on steps moving in the singular $\langle 10\bar{1} \rangle$ direction, which results in a more isotropic step velocity.

In Figures 9 and 10 we compare the flow rate dependencies of the Fourier spectra, averaged growth rate, and step velocity for the pure and the dimer-added solutions. All kinetics data in these figures were obtained during the growth of one crystal, with the growth layer source located at the lower facet corner, as shown in Figure 8. We see that, in growth from the less pure solutions, the fluctuation amplitude increases at about half the flow rate at which this increase is observed in the pure solutions. R_{avg} and v_{avg} decrease with increasing u even at the lowest flow rates. Moreover, growth cessation is reached at $u \approx 800$ μm/s at the higher $\sigma = 1.4$ (Figure 10a) and at $u \approx 1000$ μm/s at the lower $\sigma = 1.0$ (Figure 10b), i.e., at about half to one-third the flow rate at which cessation occurred in the pure solution. These observations strongly support the proposed

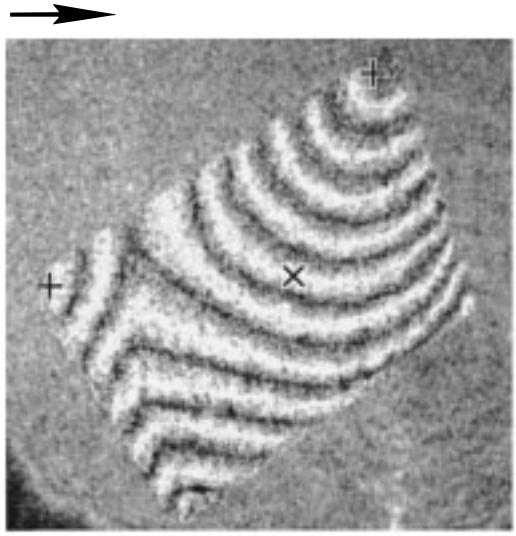

Figure 11. Representative morphology of the facet during the recording of the kinetic curves shown in Figure 12. Supersaturation $\sigma = 1.4$ ($T = 22$ °C), flow velocity $u = 105$ μm/s in direction indicated by arrow, growth from lysozyme solution containing 1% covalently bound lysozyme dimer. +, locations of layer generation; ×, location of growth kinetics monitoring.

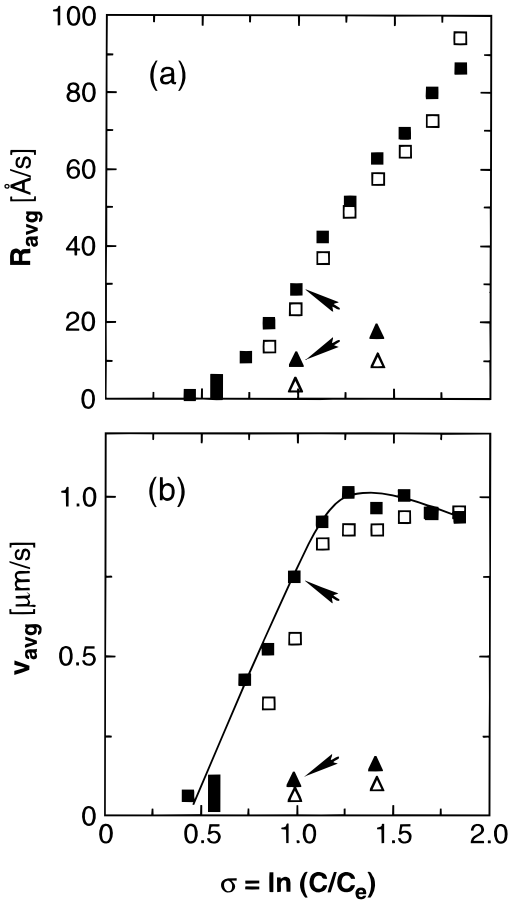

Figure 12. Supersaturation dependence of the normal growth rate (a) and step velocity (b) averaged over periods of the order 1 h. Growth from solution containing 1% lysozyme dimer. (■, ▲) $u = 105$ μm/s; (□, △) $u = 305$ μm/s; (■, □) series of measurements at the end of run, representative growth morphology is shown in Figure 11; (▲, △) measurements at earlier stages of growth of same crystal. Curve in (b) presents data fit to ■ according to (8); for parameters see text. Arrows indicate conditions for which the fluctuation characteristics are displayed in Figure 13a,b.

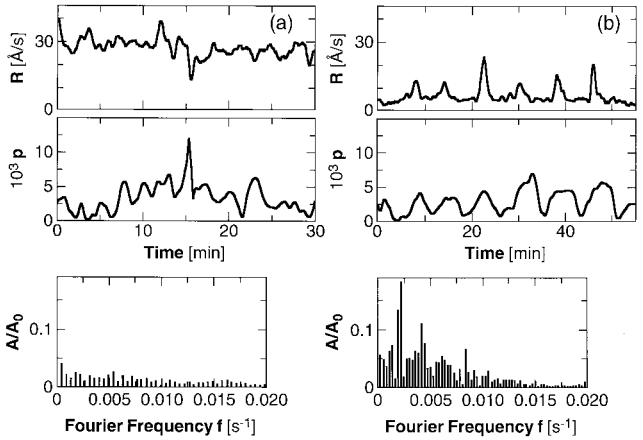

Figure 13. Traces of normal growth rate R, vicinal slope p, and Fourier spectra of R corresponding to the points marked by arrows in Figure 12 at $\sigma = 1.0$ ($T = 25$ °C) and $u = 105$ μm/s.

mechanism of increase in fluctuation amplitude due to enhanced supply of impurities to the interface, followed by their adsorption at kinks.

4.3. Growth Rate Effects on Time-Dependent Impurity Adsorption. Time-dependent impurity adsorption is a crucial assumption in the mechanisms for impurity-induced step bunching and kinetics fluctuations at high rates of convective transport. If the response of the step kinetics to the enhanced supply of impurities is weakened during growth with high R_{avg}, this would indicate impurity adsorption with characteristic times comparable to the average terrace exposure times.

To test these possibilities, we determined $R_{avg}(\sigma)$ and $v_{avg}(\sigma)$ at two flow rates during growth of a (101) face from a solution containing ~1% lysozyme dimer. The morphology of this face is depicted in Figure 11. The choice of the flow rates was based on the following considerations. As shown in Figure 7c, at the lower velocity used, $u = 105$ μm/s, $v_{avg}(u)$ reaches a maximum; above, we have interpreted this in terms of interfacial solute replenishment while the interfacial impurity concentration is still low. On the other hand, the higher velocity $u = 305$ μm/s is in the region of growth deceleration and, as shown by Figure 7a, without impurity-induced increase in the fluctuation amplitudes. The higher u chosen allows us to separate step deceleration due to impurity adsorption at kinks from that caused by deceleration amplified by impurity-induced step bunching.[30]

The $R_{avg}(\sigma)$ and $v_{avg}(\sigma)$ dependencies in Figure 12 show that at all supersaturations faster flow results in lower step velocity. The decrease in v at the higher flow rate is much greater if R is lower: at $R \approx 20$ Å/s, $\Delta v/v$ is about 30%, while at $R \approx 10$ Å/s v decreases to about half its original value. From this growth rate-dependent deceleration of step motion at higher flow rate, we conclude that the adsorption of the convection-supplied impurities on the terraces occurs with characteristic times comparable to the exposure times of the terraces.

It should be emphasized that the growth rates and step velocities in Figure 12 are significantly higher than in any previous measurements in our laboratory even with material without dimer addition.[5] These values of R and v are also higher than those obtained at earlier stages of growth of the same crystal, during which the crystal was smaller and the growth layers were generated by other dislocation sources. For comparison, typical R_{avg} and v_{avg} values measured at $\sigma = 1.0$ and 1.4 on the smaller crystal are plotted in Figure 12.

The observed $v_{avg}(\sigma)$ dependence is well reproduced by the relation

$$v_{avg} = \frac{\beta\Omega C_e(C/C_e - 1)}{1 + kp_{avg}} \quad (8)$$

with the kinetic coefficient $\beta = 2 \times 10^{-3}$ cm/s and step field overlap parameter $k = 500$. This is shown by the curve in Figure 12b, which was calculated from (8) with these parameters and the $p_{avg}(\sigma)$ dependence recorded in parallel with R_{avg} and v_{avg} in Figure 12. The value of k agrees well with previous determinations for the same system (see discussion in ref 20). However, the value of β is about 10−50 times higher than previously determined.[25,32,33,41,42] Note that in these earlier works a different definition of the supersaturation in (8) was used, which leads to a β value higher by about 5 times from the one determined based on eq 8. This high β value is comparable to the step kinetic coefficient for some inorganic crystal growth systems[15,43,44] and exceeds all published kinetic coefficients for proteins[6,45] by 1−2 orders of magnitude.

To rationalize this high β value, we recall that in a previous study we have seen that, as a crystal grows, the dislocation source activity drops.[25] We related this decrease to diverging lines of bunched dislocations, leading to fewer dislocations being within a distance ρ_c corresponding to the radius of a critical 2D nucleus whence they act as a joint growth layer source.[46,47] Furthermore, as we have discussed in connection with our numerical simulations of step bunching,[20] unsteadiness in step source activity acts as a trigger for the bunching that underlies the growth rate fluctuations. As the number of dislocations in a growth layer source decreases with crystal size, it is reasonable to expect that the layer generation becomes more regular and the step density perturbations weaken. This results in reduced step bunching in the generated step train. It appears that such a step train spreads with higher v_{avg} than a step train with higher step bunches.

This hypothesis is supported by Figure 13, which presents the fluctuation patterns corresponding to the pair of R and v measurements at $u = 105$ μm/s and $\sigma = 1.0$ marked by arrows in Figure 12. We see that faster growth rate and step velocity are associated with lower step bunching and growth rate fluctuations. Further experimental evidence and theoretical considerations that connect the unsteady growth characteristics to the average values of the kinetic variables will be provided in a forthcoming paper.[30]

5. Summary and Conclusions

We have shown that Fourier spectra of time traces of growth rates are governed by the solution conditions and the activity of the growth layer source and can be used to characterize the unsteady crystal growth kinetics. Utilizing this characterization tool, our studies have revealed the following major points on the growth kinetics of lysozyme:

1. At lower flow rates, enhanced solute supply to the interface results in acceleration of step velocity and growth rate by about 10%.

2. More rapid convective transport to the interface leads to a reduction of the kinetics fluctuations (step bunching). This observation corroborates our previous conclusion that the fluctuations and step bunching represent an intrinsic response of the system of coupled transport and interfacial processes to perturbations in step density.[17,20] Since kinetic unsteadiness causes inhomogeneities in the crystal, these studies also support the rationale for system-dependent effects of the changes in transport conditions on the quality of solution-grown crystals.[17,48]

3. Solution flow also enhances the interfacial supply of impurities that are incorporated into the crystal. If the characteristic adsorption times of such impurities are comparable to the exposure times of the terraces between steps, impurity-induced step bunching occurs even in systems with impurity levels as low as 0.01%, i.e., at purity levels which are very difficult to obtain and characterize in biochemical preparations. Similar to the intrinsic bunching, this impurity-induced macrostep formation is detrimental for crystal homogeneity.

4. At low supersaturations and, hence, growth rates, convection-enhanced impurity transport can result in complete growth cessation. This observation provides an unambiguous explanation for earlier observations of cessations in growth from unstirred[49] and recirculating[50] solutions.

5. Earlier observations of "slow growth kinetics" with lysozyme and, possibly, other proteins appear to be the result of step bunch formation in response to nonsteady step generation. In growth through layer spreading from relatively steady step sources, protein incorporation kinetics can be associated with rates that approach those of inorganic systems.

Acknowledgment. This paper has greatly benefited from numerous discussions with A. A. Chernov and J. I. D. Alexander. L. Carver expertly prepared the figures. This work was supported by the Microgravity Science and Applications Division of NASA (Grant NAG8-950 and NAG8-1168) and the State of Alabama through the Center for Microgravity and Materials Research at the University of Alabama in Huntsville.

References and Notes

(1) Littke, W.; John, Chr. *Science* **1984,** *225*, 203; *J. Cryst. Growth* **1986,** *76*, 663.
(2) Day, J.; McPherson, A. *Protein Sci.* **1992,** *1*, 1254.
(3) DeLucas, L. J.; et al. *J. Cryst. Growth* **1994,** *135*, 183. Long, M. M.; Bishop, J. B.; Nagabhushan, T. L.; Reichert, P.; Smith, G. D.; DeLucas, L. J. *J. Cryst. Growth* **1996,** *168*, 233.
(4) McPherson, A. *Proceedings of the Eighth European Symposium on Materials and Fluids Sciences in Microgravity, 1992, ESA SP-333*, 619; *J. Phys. D: Appl. Phys.* **1993,** *26*, 104.
(5) Rosenberger, F.; Vekilov, P. G.; Muschol, M.; Thomas, B. R. *J. Cryst. Growth* **1996,** *168*, 1.
(6) Malkin, A. J.; Kuznetsov, Yu. G.; Glantz, W.; McPherson, A. *J. Phys. Chem.* **1996**, *100*, 11736. McPherson, A.; Malkin, A. J.; Kuznetsov, Yu. G. *Structure* **1995**, *3*, 759.
(7) Pusey, M.; Witherow, W.; Naumann, R. *J. Cryst. Growth* **1988,** *90*, 105.
(8) Lin, H.; Rosenberger, F.; Alexander, J. I. D.; Nadarajah, A. *J. Cryst. Growth* **1995**, *151*, 153.
(9) Rosenberger, F. *J. Cryst. Growth* **1986,** *76*, 618.
(10) Ataka, M.; Tanaka, T. *Biopolymers* **1986**, *58*, 337.
(11) Weber, P. In *Advances in Protein Chemistry;* Afinsen, C. B., Richards, F. M., Edsal, J. T., Eisenberg, D. S., Eds.; Academic Press: New York, 1991; Vol. 41, p 1.
(12) Frank, F. C. In *Growth and Perfection of Crystals*; Doremus, R. H., Roberts, B. W., Turnbull, D., Eds.; Chapman and Hill: London, 1958; p 411.
(13) Chernov, A. A.; Parvov, V. F.; Kliya, M. O.; Kostomarov, D. V.; Kuznetsov, Yu. G. *Sov. Phys.−Crystallogr.* **1981,** *26*, 640.
(14) Chernov, A. A.; Malkin, A. J. *J. Cryst. Growth* **1988**, *92*, 432.
(15) Rashkovich, L. N. *KDP−Family of Crystals*; Adam Hilger: Bristol, 1991.
(16) Vekilov, P. G.; Monaco, L. A.; Rosenberger, F. *J. Cryst. Growth* **1995,** *146*, 289.
(17) Vekilov, P. G.; Alexander, J. I. D.; Rosenberger, F. *Phys. Rev.* **1996,** *E 54*, 6650.
(18) Gray, P.; Scott, S. K. *Chemical Oscillations and Instabilities. Nonlinear Chemical Kinetics*; Clarendon Press: Oxford, 1990.
(19) Noyes, R. M.; Fields, R. J. *Annu. Rev. Phys. Chem.* **1974,** *25*, 95.
(20) Vekilov, P. G.; Lin, H.; Rosenberger, F. *Phys. Rev.* **1997,** *E55*, 3202.
(21) Thomas, B. R.; Vekilov, P. G.; Rosenberger, F. *Acta Crystallogr.* **1996,** *D52*, 776.

(22) Thomas, B. R.; Vekilov, P. G.; Rosenberger, F. *Acta Crystallogr. D* **1998**, *54*, 226.
(23) Vekilov, P. G.; Rosenberger, F. *J. Cryst. Growth* **1998**, *186*, 251.
(24) From software package Mathcad by MathSoft, Cambridge, MA.
(25) Vekilov, P. G.; Rosenberger, F. *J. Cryst. Growth* **1996**, *158*, 540.
(26) Levich, V. G. *Physicochemical Hydrodynamics*; Prentice-Hall: Englewood Cliffs, 1962.
(27) Chernov, A. A. *Sov. Phys.−Uspekhi* **1961**, *4*, 116.
(28) van der Eerden, J. P. *J. Cryst. Growth* **1982**, *56*, 174.
(29) Yoo, H. D.; Wilcox, W. R.; Lal, R. B.; Trolinger, J. D. *J. Cryst. Growth* **1988,** *92*, 10.
(30) Vekilov, P. G.; Alexander, J. I. D.; Rosenberger, F. *Phys. Rev. Lett.*, submitted for publication.
(31) Vekilov, P. G.; Chernov, A. A., manuscript in preparation.
(32) Vekilov, P. G.; Ataka, M.; Katsura, T. *J. Cryst. Growth* **1993,** *130*, 317.
(33) Vekilov, P. G. *Prog. Cryst. Growth Charact*. **1993**, *26*, 25. Vekilov, P. G.; Ataka, M.; Katsura, T. *Acta Crystallogr*. **1995,** *D51*, 207.
(34) Miyashita, S.; Komatsu, H.; Suzuki, Y. *Jpn. J. Appl. Phys.* **1993**, *32*, 1855.
(35) Miyashita, S.; Komatsu, H.; Suzuki, Y.; Nakada, T. *J. Cryst. Growth* **1994**, *141*, 419.
(36) van der Eerden, J. P.; Müller-Krumbhaar, H. *Electrochim. Acta* **1986,** *31*, 1007.
(37) van der Eerden, J. P.; Müller-Krumbhaar, H. *Phys. Rev. Lett*. **1986**, *57*, 2431.
(38) Bliznakov, G. *Adsorption et Croissance Cristalline*; Centre National de la Recherche Scientifique: Paris, 1965; p 300; *Fortsch. Min*. **1958**, *36*, 149.
(39) Chernov, A. A. *Modern Crystallography;* Springer: Berlin, 1984; Vol. III, p 161.
(40) Cabrera, N.; Vermileya, D. A. In *Growth and Perfection of Crystals*; Doremus, R. H., Roberts, B. W., Turnbull, D., Eds; Wiley: New York, 1958; p 393. Voronkov, V. V.; Rashkovich, L. N. *Soviet Phys.−Crystallogr*. **1992**, *37*, 289; *J. Cryst. Growth* **1994,** *144*, 107.
(41) Vekilov, P. G.; Monaco, L. A.; Rosenberger, F. *J. Cryst. Growth* **1995,** *156*, 267.
(42) Lin, H.; Vekilov, P. G.; Rosenberger, F. *J. Cryst. Growth* **1996**, *158*, 552.
(43) Chernov, A. A. *Z. Phys. Chem. Leipzig* **1988**, *269*, 941; *Contemp. Phys*. **1989**, *30*, 251.
(44) Görnert, P.; Voigt, F. In *Current Topics in Materials Science;* Kaldis, E., Ed.; North-Holland: Amsterdam, 1984; p 1.
(45) Chernov, A. A.; Komatsu, H. In *Science and Technology of Crystal Growth*, van der Eerden, J. P., Bruinsma, O. S. L., Eds.; Kluwer Academic Publishers: Dordrecht, 1995; pp 67, 329.
(46) Burton, W. K.; Cabrera, N.; Frank, F. C. *Philos. Trans. R. Soc. London, Ser. A* **1951,** *243*, 299.
(47) Chernov, A. A.; Rashkovich, L. N.; Mkrtchan, A. A. *J. Cryst. Growth* **1985,** *74*, 737.
(48) Rosenberger, F.; Vekilov, P. G.; Lin, H.; Alexander, J. I. D. *Microgravity Sci. Technol.* **1997**, *10*, 29.
(49) Kam, Z.; Shore, H. B.; Feher, G. *J. Mol. Biol.* **1978,** *123*, 539. Feher, G.; Kam, Z. In *Methods in Enzymology;* Wyckoff, H. W, Hirs C., H. W., Timasheff, S. N., Eds.; Academic Press: New York, 1985; Vol. 114, p 77.
(50) Nyce, T. A.; Rosenberger, F. *J. Cryst. Growth* **1991**, *110*, 52.